Journal of Alloys and Compounds 509 (2011) 1630–1635

Contents lists available at ScienceDirect

Journal of Alloys and Compounds

journal homepage: www.elsevier.com/locate/jallcom

Mechanism of the α-to-β phase transformation in the $LaNi_5$–H_2 system

E.M[ac]A. Gray[a,*], T.P. Blach[a], M.P. Pitt[a], D.J. Cookson[b,1]

[a] Queensland Micro and Nanotechnology Centre, Griffith University, Nathan 4111, Brisbane, Australia
[b] Australian Synchrotron Research Program, Bldg 434, Advanced Photon Source, Argonne, IL 60439, USA

ARTICLE INFO

Article history:
Received 17 August 2010
Received in revised form 5 November 2010
Accepted 11 November 2010
Available online 21 November 2010

Keywords:
Hydrides
Hydrogen absorption
Phase transformation kinetics
X-ray diffraction

ABSTRACT

High-energy synchrotron in situ X-ray powder diffraction has been used to elucidate the mechanism of the hydriding phase transformation in a $LaNi_5$ model hydrogen storage intermetallic in real time. The transformation proceeds at 10 °C via the transient growth of an interfacial phase, the γ phase, with lattice parameters intermediate between those of the α (dilute solid solution) and β (concentrated hydride) phases. The γ phase forms to partially accommodate the 24% change in unit cell volume between the α and β phases during hydriding and dehydriding. The α, γ and β phases coexist at the nanoscopic level.

1. Introduction

$LaNi_5$–H_2 is an important model system for understanding the absorption of atomic hydrogen by metals and has been much studied in relation to hydrogen storage, particularly in nickel–metal-hydride batteries. As the phase transformation between the dilute solid solution (α-$LaNi_5H_x$: $x \leq 0.5$ approximately) and the concentrated hydride (β-$LaNi_5H_x$: $x \geq 6$ approximately) is the basic means by which hydrogen is stored and released, knowledge of the transformation mechanism is vitally important.

Numerous neutron diffraction and synchrotron X-ray studies of the α and β phases have been made to establish their crystallographic parameters [1–5] and investigate their microstructures, particularly with respect to the dislocations that are generated [6–10] when the β phase is formed for the first time [11–20]. Diffraction showed that a lattice expansion corresponding to a 24% volume increase occurs when the α phase transforms to the β phase.

In situ hydrogenation allows the system to be studied at global hydrogen concentrations between those of the pure phases. The first in situ neutron-diffraction study of the $LaNi_5$–H_2 system [21] showed that the lattice parameters and local strain depend strongly on the proportions of the α and β phases, demonstrating that they are in nanoscale mechanical contact via an interface which has at least partial coherence. Accommodation of the volume difference between the α and β phases thus proves to be the basic determinant of the mechanism of the phase transformation. The volume difference is also a significant empirical factor in the longevity of Ni–metal-H batteries [22], providing another reason to fully understand the mechanism of the α-to-β phase transformation.

In the conventional picture (e.g. [23]), the α and β phases coexist with constant composition and variable phase proportions at notionally constant pressure, leading to the well-known absorption and desorption pressure plateaux[2] in the pressure-composition isotherm observed for this and many other metal–hydrogen systems. At temperatures above about 80 °C, however, a third hydride phase (γ-$LaNi_5H_x$: $x \approx 3$)[3] [24–26] has been observed in apparent coexistence with both the α and β phases in a significant range of pressure at constant temperature [24,25]. The occurrence of γ-like intermediate phases has also been reported in ACo_5H_y (A = La, Ce and Pr) [27] and $CaNi_5H_y$ [28,29].

In the most recent diffraction study of the $LaNi_5$–H_2 system by Joubert et al. [30], it was shown using in situ synchrotron X-ray diffraction that the γ phase occurs transiently even at room temperature after the β phase has been formed once, thus confirming the observation by Kisi and Gray [31] of a small amount of transient diffuse intensity between the $(1\,0\,1)_\alpha$ and $(1\,0\,1)_\beta$ Bragg peaks when the transformation was followed in real time with laboratory

* Corresponding author. Tel.: +61 7 3735 7240; fax: +61 7 3735 7656.
E-mail address: E.Gray@griffith.edu.au (E.M[ac]A. Gray).
[1] Now at Australian Synchrotron, Clayton 3168, Australia.

[2] "Plateau" refers to the nominally horizontal portion of the absorption or desorption pressure-composition isotherm (by convention graphed as pressure against *H*/*M*), indicating according to the Gibbs phase rule the coexistence of two phases in equilibrium at constant chemical potential.
[3] Although this phase is referred to as the β phase by its discoverers [24], we reserve the "β" designation for pure $LaNi_5H_6$.

0925-8388/$ – see front matter © 2010 Elsevier B.V. All rights reserved.
doi:10.1016/j.jallcom.2010.11.083

X-rays. The emphasis of Joubert et al. was on the microstructural evolution during the phase transformation, through interpretation of the systematic Bragg peak broadening as a function of the phase proportions. The role of the γ phase in the transformation was not explained.

Some important questions thus arise about the hydriding and dehydriding phase transformations: why does a third hydride phase occur at all, why transiently at room temperature, and under what conditions?

In this work our focus was on the mechanism of the α-to-β transformation and how the γ phase contributes to it. We studied the transformation mechanism in the most direct way, via the crystallographic parameters of the transforming phases. The large unit cell expansion from the α to the β phase in the $LaNi_5$–H_2 system means that the transformation is readily studied with in situ diffraction. We used high-energy synchrotron X-ray diffraction to follow the transformation mechanism in situ and in real time, in response to an increase or decrease of the surrounding H_2 gas pressure.

2. Experimental details

Extreme care was taken to avoid the accidental appearance of the γ phase, owing to uncontrolled temperature increase during the exothermic hydrogen absorption, and any spurious triple coexistence of the α, β and γ phases, owing to macroscopic spatial inhomogeneity of the phase proportions, caused by temperature gradients in the sample [31–33], which *prima facie* could be the origin of previous reports of the triple coexistence of hydride phases [24,25]. A stainless-steel X-ray pressure cell was used, described in detail elsewhere [34]. This has a disk-shaped sample space, 0.5 mm thick and 16 mm in diameter, sandwiched between heavy Be beam windows that also serve to remove the heat of transformation (approximately 30 kJ/mol-H_2) and prevent temperature gradients in the sample. A soft copper ring with a cut-out for gas ingress was used to confine the sample to a central space approximately 12 mm in diameter by compressing it between the Be windows. The temperature of the sample cell was adjusted by a Peltier-effect heat pump and the cell was surrounded by a vacuum shroud with Kapton® beam windows. This setup achieves far tighter temperature stability and uniformity within the sample than is possible with the more popular reflection or capillary sample geometries: in reflection geometry the temperature of the free sample surface illuminated by the beam is controlled only indirectly by heat flow through the full sample depth to the sample holder [31]; in a capillary [30] the removal of heat is basically by conduction through the surrounding gas, which is a very inefficient process for a line heat source of small diameter. In our cell the thick, thermally conducting Be windows that contain the sample are connected to a massive heat sink (the cell body) [34]. The cell temperature was controlled at 10.0 ± 0.1 °C for this experiment, to minimise the possibility of any local temperature excursion during rapid absorption causing the appearance of the γ phase, and to slow the reaction compared to room temperature and so allow longer data collection times for improved diffraction pattern quality.

The sample cell was close-coupled to a small calibrated hydrogenation apparatus equipped with a remotely operated valve for admitting hydrogen gas to the sample space when the X-ray beam was on. This arrangement allowed the global hydrogen content of the sample to be calculated during the experiment from the hydrogen gas pressure for comparison to the phase proportions determined by quantitative phase analysis. Extremely pure hydrogen gas was desorbed from an integrated hydride source. In contrast to Ref. [30], where a high and relatively constant driving pressure of 15 bar was applied to the hydrogenation reaction, our hydrogenation apparatus was operated in isochoral (or Sieverts) mode, by admitting hydrogen to the sample cell from a pre-loaded reference volume and allowing the system to approach equilibrium under a constant-volume constraint. This approach facilitated halting the absorption or desorption reaction in the two-phase region if desired. We therefore used much smaller driving pressures than Joubert et al. [30].

The sample material was closely stoichiometric powdered $LaNi_5$ ($CaCu_5$ structure type, *P*6/*mmm* space group, La site 1*a*, Ni sites 2*c*, 3*g*) from Santoku Corporation, Japan (alloy MCR-51202). Two samples were studied, sample A with mass 0.798 g and sample B, more loosely packed in the cell, with mass 0.400 g. The samples were prepared by executing five absorption–desorption cycles in the X-ray cell at room temperature to reach a stable microstructure [20]. The initial hydrogen absorption ("activation") powders the brittle intermetallic and so contributes to good powder averaging.

Diffraction patterns were recorded in transmission mode on ChemMatCARS at the Advanced Photon Source, Argonne National Laboratory, at a wavelength of 0.400 Å (31 keV X-ray energy). The beam footprint at the sample was set to 100 μm × 100 μm or 50 μm × 50 μm to minimise the smearing effect of any temperature gradient that might have occurred despite the precautions listed above. Diffraction patterns were recorded with a Bruker 6000 CCD image collector. The detector was moved off the beam axis to give a range of Bragg angles from 3° to 17° in 2θ. The Debye–Scherrer diffraction rings were integrated in software to achieve good powder averaging with a stationary sample and corrected for the "tan-θ" effect of the flat detector to give line profiles. Pattern collection times of 5–20 s gave excellent resolution of the kinetics of the phase transformation. Rietveld profile analysis was conducted with the Rietica software [35], with a simple model of dislocation scattering [12] applied to the strong anisotropic broadening of the Bragg peaks that is characteristic of hydrogen-cycled $LaNi_5$. No attempt was made to extract information about dislocations from the diffraction data because the data are of medium resolution and the peak broadening includes unknown contributions from the elastic strains at the α–γ and γ–β interfaces. The γ phase was modelled in the *P*321 space group [36].

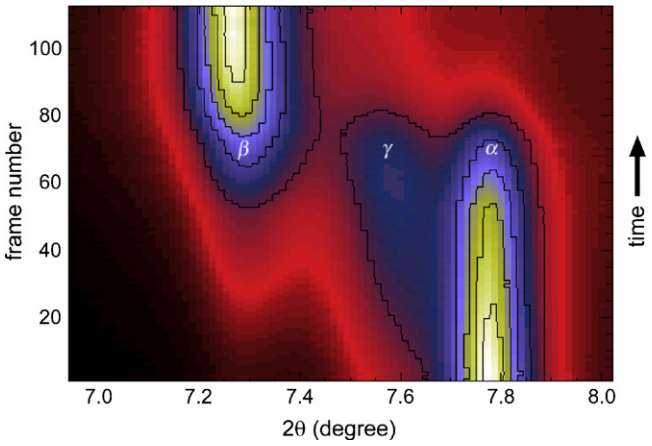

Fig. 1. Detail from the kinetic X-ray diffraction pattern sequence recorded while absorbing hydrogen from $H/M = 0.17$ to 0.85 in the illuminated voxel of sample A. The Bragg peaks shown are for the (1 0 1) reflections from the α, γ and β phases.

Only local values of *H*/*M*, the atomic ratio of hydrogen atoms to host metal atoms, are quoted in this paper. These were estimated from the diffraction pattern by quantitative phase analysis, assuming *H*/*M* values for the coexisting α, γ and β phases of 0.1, 0.5 and 0.9, respectively. These values of *H*/*M* therefore apply to the illuminated voxel (typically 100 μm × 100 μm × 500 μm) of the sample. As detailed below, the global value of *H*/*M*, averaged over the entire sample volume and calculated from the hydrogen pressure, was unexpectedly found to be generally different to the local value in the footprint of the X-ray beam, owing to spatial inhomogeneity of the phase proportions arising in a pressure gradient, not a temperature gradient.

3. Results

Fig. 1 depicts the result for sample A of applying a relatively large step in hydrogen pressure from 1.50 bar to 4.77 bar, which drove the local hydrogen content in the 100 μm × 100 μm footprint of the X-ray beam from a starting position at $H/M = 0.17$, near the beginning of the absorption plateau, to $H/M = 0.85$, or nearly pure β phase, at a final pressure of 2.48 bar. In this sequence, 112 frames of data were recorded with the beam illuminating only the centre of the sample, initially 20 s apart, on a time scale that stretched in roughly logarithmic fashion over 2 h. For clarity, only the (1 0 1) Bragg peaks are shown, as they exhibit the α, β and γ phases well-separated in 2θ. Beginning at the bottom of Fig. 1, $(1\,0\,1)_\gamma$ grows on the side of $(1\,0\,1)_\alpha$ at $2\theta = 7.8°$ and moves towards larger cell dimensions as $(1\,0\,1)_\beta$ emerges near $2\theta = 7.3°$. The γ and α phases disappear together as $(1\,0\,1)_\beta$ grows. It is obvious by inspection of these diffraction profiles that much more γ phase was formed in this sample than was observed by Joubert et al. [30].

Because the value of *H*/*M* in the illuminated voxel of sample A did not agree with the global value calculated from the hydrogen pressure, we loaded and activated in situ a new sample, sample B, which was packed to only about half the effective density of sample A, to give faster hydrogen flow though the sample. On this occasion, starting from a hydrogen pressure of 0.97 bar (pure α phase) and stepping to just 2.25 bar caused the phase transformation in the illuminated voxel in the centre of sample B to largely complete within 1 min (Fig. 2), reaching a final pressure of 1.57 bar after 17 min. This result demonstrates the fast kinetics achievable with $LaNi_5$, even at lowered temperature and with a very small pressure

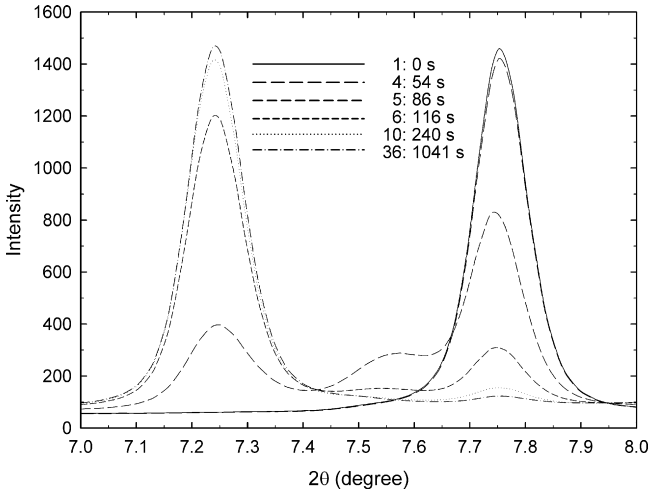

Fig. 2. Demonstration of the fast kinetics of sample B at 10 °C with low pressure drive. Legend indicates frame number and corresponding time from admission of hydrogen. The phase transformation was largely completed in 62 s between frames 4 and 10, slowing thereafter.

drive, when the heat of transformation is effectively removed by excellent heat sinking. In contrast, Joubert et al. [30] observed the transformation to take place in approximately the same time with a 15-bar driving pressure, starting at ambient temperature. A delay of about 1 min was noted before the transformation began, suggesting that the phase transformation was progressing along the sample rather than occurring uniformly everywhere.

To understand the disagreement between the global and local phase proportions in our experiment, we performed a diffraction survey of sample B after allowing an absorption sequence from an initial system pressure of 1.87 bar to a final pressure of 1.37 bar to evolve and settle for a total of 75 min. Then the beam footprint was reduced to 50 μm × 50 μm and the sample cell was translated in two dimensions perpendicular to the beam axis, in 500-μm steps. The result is shown in Fig. 3. A frozen transformation wave is apparent, originating at the gas inlet, crossing the sample and leaving pure β phase in its wake. It is clear that this compositional inhomogeneity is related to the availability of hydrogen, not to any temperature distribution in the sample, which would reflect the circular symmetry of the cell. We rationalise this result as follows. The intrinsic kinetics of $LaNi_5$ is so fast that powder grains near the hydrogen inlet absorbed to β phase before the hydrogen had flowed across the entire sample. This lowered the hydrogen pressure, owing to the isochoral constraint, thus decreasing the pressure drive for the transformation in more distant parts of the sample below the quasistatic transformation pressure, halting the hydride reaction and producing the frozen macroscopic inhomogeneity of the phase proportions shown in Fig. 3. In the original work on inhomogeneity of the phase proportions in $LaNi_5$–H_2, Pons and Dantzer [32] did not need to account for hydrogen flow through the packed hydride bed to model their experimental results, as the evolution of the phase proportions was controlled by temperature gradients caused by the poor thermal conductivity of the powdered sample. In the present situation, the heat sinking of the hydride bed is so good that the reverse is true and the result is controlled by hydrogen flow through the space between the metal/metal-hydride particles. The 24% by volume swelling during the α-to-β transformation in $LaNi_5$–H_2 clearly exacerbates this effect, further choking the hydrogen flow across the sample during absorption.

Fig. 4 details the initiation of the α-to-β phase transformation in sample B, starting in pure α phase and applying a much smaller pressure change than in Fig. 1, from 1.39 bar to 1.98 bar, to slow the transformation, and with a shorter 5-s diffraction pattern collection time. The inset highlights the diffracted intensity around the $(1\,0\,1)_\beta$ position. The sequence of events is that, as the solid-solution α phase begins to absorb H atoms, $(1\,0\,1)_\alpha$ rapidly moves to a lower angle between frames 2 and 3, before $(1\,0\,1)_\gamma$ begins to grow on its lower wing in frames 4–6. Not until frame 9 is there any appreciable intensity at the $(1\,0\,1)_\beta$ position. After 39 min the system pressure had settled to 1.42 bar and the transformation had stopped.

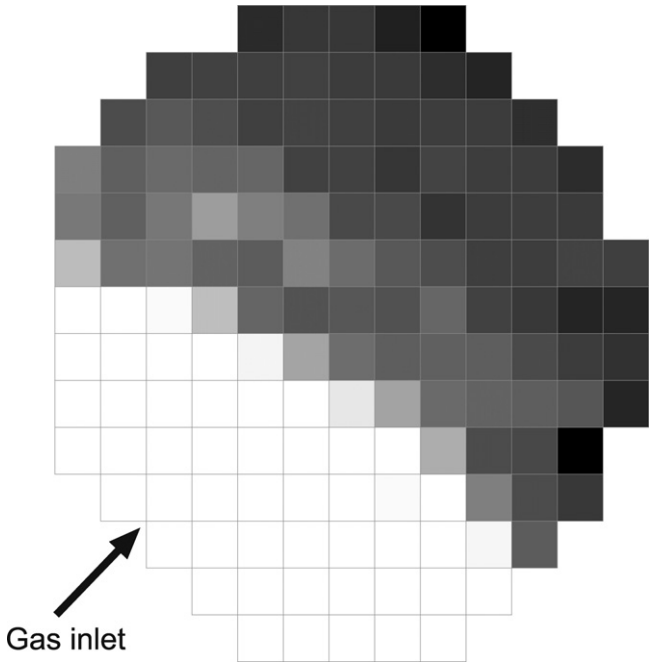

Fig. 3. β-Phase fraction mapped across sample B in 500-μm increments at the end of an isochoral absorption step, starting from the fully desorbed (pure α phase everywhere) condition. 100% β phase is represented as white and 0% β phase is represented as black. Note the α–β transformation wave crossing the sample from lower-left to upper-right, preceded by a mixture of the α, β and γ phases. The fraction of γ phase is greatest immediately ahead of the transformation.

A second absorption step from 1.42 bar to 1.87 bar saw the α-to-β transformation largely complete, analogous to Fig. 1 for sample A,

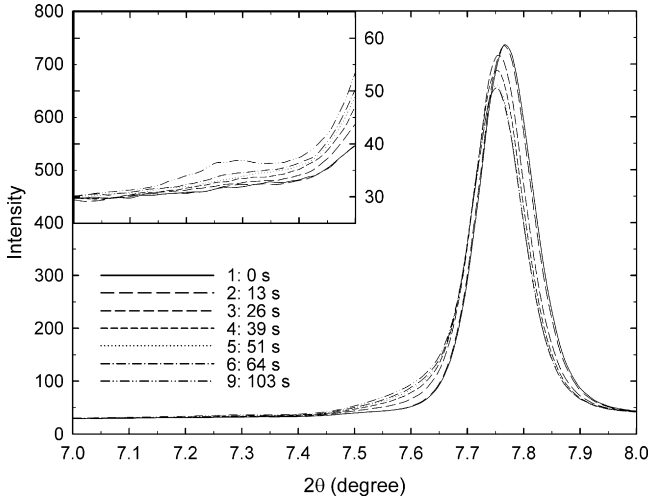

Fig. 4. Short-time evolution of the (1 0 1) Bragg peaks from the α, γ and β phases during hydrogen absorption by sample B under low pressure drive, beginning in pure α phase. Legend indicates frame number and corresponding time from admission of hydrogen. Significant $(1\,0\,1)_\gamma$ intensity develops on the low-angle side of $(1\,0\,1)_\alpha$ before any intensity is observed at the $(1\,0\,1)_\beta$ position.

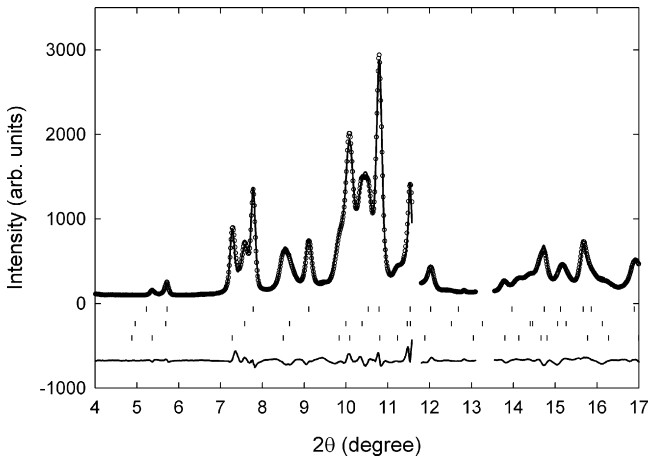

Fig. 5. Diffraction profile recorded at $t = 1781$ s during the kinetic sequence depicted in Fig. 1 for sample A. Circles: experimental points. Line: fit to three-phase model. Difference profile shown at bottom. Reflection markers from top to bottom are for the α, γ and β phases. Be window peaks have been cut out of the profile. Agreement indices: $R_p = 3.835$, $R_{wp} = 5.477$, $\chi^2 = 1.245$, $R_B(\alpha) = 2.25$, $R_B(\gamma) = 1.35$, $R_B(\beta) = 2.05$.

except that significantly less γ phase was formed, a point discussed below.

Entirely analogous behaviour was observed during desorption, in which the pressure drive was necessarily low because of the low quasistatic desorption pressure of approximately 0.9 bar: the γ phase was seen to grow from the β phase and then transform to the α phase. The amount of γ phase formed during desorption was comparable to the amount formed during absorption with a comparable pressure drive.

Rietveld profile analysis was performed on selected entire diffraction profiles from the sequence depicted in Fig. 1. Fig. 5 shows a diffraction profile from the middle of this time sequence. Fig. 6 shows the time evolution of the phase proportions corresponding to Fig. 1, calculated from the Rietveld scale factors, and the lattice parameters. As observed for the static occurrence of the γ phase at elevated temperatures [24–26], and its transient occurrence at room temperature [30], a of the γ phase is closer to that of the β phase (Fig. 6(b)) while c of the γ phase is closer to that of the α phase (Fig. 6(c)).

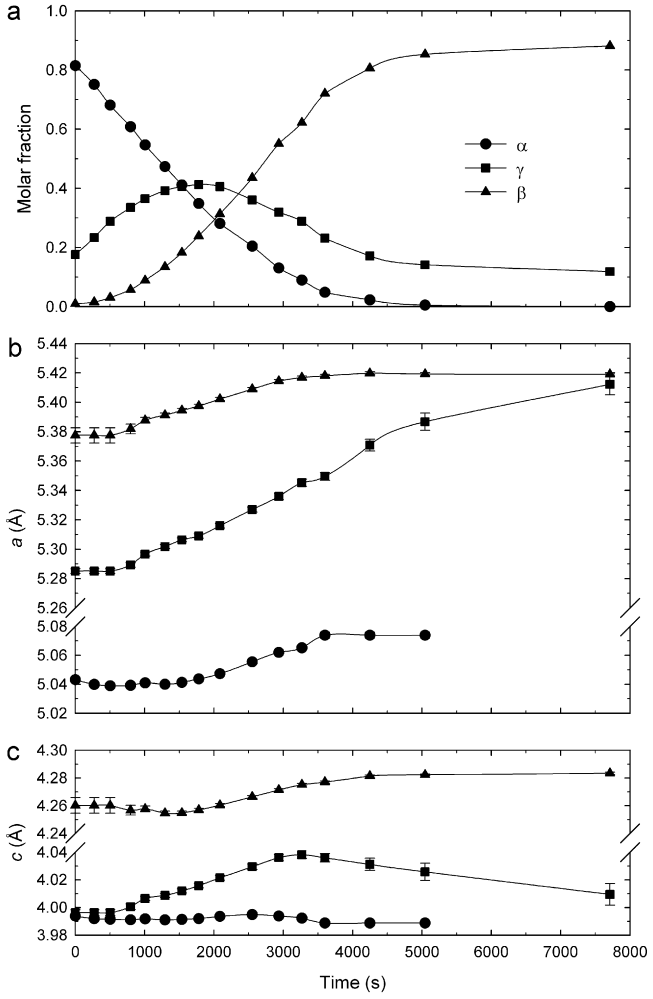

Fig. 6. Phase proportions (a) and lattice parameters (b), (c) determined by Rietveld profile refinement of selected diffraction profiles from the absorption sequence depicted in Fig. 1 for sample A.

4. Discussion

The results in Figs. (1)–(6) allow immediate clarification of the nature of the phase transformation in the $LaNi_5$–H_2 system.

The absolute values of the lattice parameters (Figs. 6(b) and (c)) confirm that the γ phase is (i) distinct from the α and β phases and (ii) the same phase as that observed at elevated temperatures, having therefore around 3H atoms per formula unit. Because of the spatially inhomogeneous phase proportions, the H content of the γ phase cannot be calculated from the refined measured phase proportions and the global value of H/M.

Contrary to the results of Joubert et al. [30], in which no change in the γ-phase lattice parameters was observed as the transformation proceeded, the sense of the γ phase stretching or contracting to accommodate the dominant coexisting phase is clearly conveyed by Fig. 6, confirming the (at least) partial coherence of the transformation. A possible reason for this discrepancy is the small illuminated voxel volume (0.005 mm^3 maximum) in our experiments, in contrast to the 5-mm length of 0.3-mm diameter capillary (0.35 mm^3) over which the inhomogeneous phase proportions were averaged in the experimental setup of Joubert et al. Inhomogeneity of the phase proportions in their setup is strongly suggested by the apparent incubation time for the desorption reaction into vacuum, when nearly 2 min elapsed before the transformation began in the illuminated sample voxel. This is just as would expected of a transformation wave progressing along the capillary from the hydrogen inlet to and then through the illuminated voxel.

Figs. 3 and 4 show that the γ phase must form before the β phase during absorption (and by analogy before the α phase during desorption). This is confirmed in Fig. 6(a) by the slow increase of the β fraction at the start of the kinetic absorption sequence, in contrast to the rapid formation of the γ phase.

Our results strongly suggest that the γ phase actually constitutes the interface between the α and β phases, forming ahead of the β phase as it ingests the α phase in absorption and *vice versa* in desorption, in sequential fashion. Given the fact that, at its peak of existence, the γ phase can actually be the dominant phase (Fig. 6(a)), the γ phase is not a conventional "interface", but this term does convey the essential connectedness of the α and β phases via the γ phase that is necessary to explain the sequential nature of the phase evolution.

Noting that the γ phase is most obvious while the interface between the α and β phases is moving rapidly, i.e. while the α and β phase proportions are changing rapidly in opposite directions (Fig. 6(a)), the time evolution of the phase proportions can be qualitatively modelled as follows. Assume that the γ phase is in fact an interfacial layer between the α and β phases and that it is required

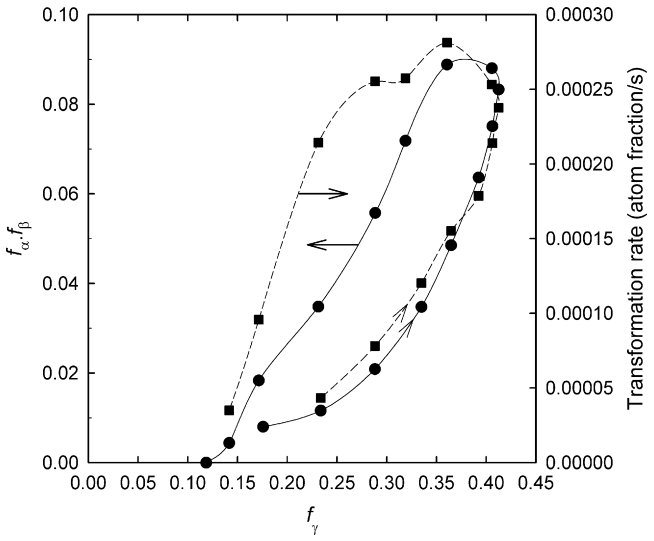

Fig. 7. Relationship of the reaction rate and product of the α and β phase proportions (f_α, f_β) to the proportion of the γ phase (f_γ), for the data of Fig. 6(a).

for the formation of the β phase during hydrogen absorption and for α formation in desorption. In the crudest approximation we assume that the volume of γ phase is simply proportional to the area of the α–β interface (γ layer area) and to the transformation rate (γ layer thickness). Representing the former by the product of the α and β phase fractions, with a maximum when $f_\alpha = f_\beta$, and the latter by the rate of formation of the β phase (during absorption) we expect $f_\gamma \sim f_\alpha f_\beta \dot{f}_\beta$. Based on the data of Fig. 6(a), Fig. 7 compares the quantities $f_\alpha f_\beta$ and $\dot{f}_\beta$ to f_γ and demonstrates a rough proportionality to both. We speculate that the hysteresis in Fig. 7 arises in dissipative mechanisms associated with the phase transformation, e.g. dislocation generation.

The maximum fraction of the γ phase observed in this study during hydrogen absorption (ca. 40 mol.%) was significantly more than was observed by Joubert et al. [30] (ca. 10%), which we explain as follows. The temperature of our sample was lower (10 °C) and tightly controlled, compared to the setup in Ref. [30] of room temperature with no control of the temperature rise caused by the exothermic H absorption, implying much slower H diffusion in our case and the need for a greater volume of γ phase to accommodate the volume difference between the α and β phases, compared to the demonstrably quicker transformation at higher temperatures. The likely compositional inhomogeneity in the form of a transformation wave progressing along the capillary in Ref. [30] would further lower the apparent fraction of γ phase when averaged over the illuminated length of capillary. In desorption, the γ-phase fractions observed in the two studies were more comparable, explained by the necessarily lower pressure drive in [30] (1 bar maximum compared to about 12 bar during absorption 2) and consequently slower transformation causing only moderate cooling of the sample.

An important question is whether or not γ phase is always present, and on this point our results are not directly conclusive. While some γ phase remained at the end of our kinetic sequences in which the phase transformation was incomplete in the illuminated voxel (Figs. 1, 4 and 6), this is an artefact of the isochoral conditions, in which the hydrogen pressure falls or rises until the driving force for the transformation disappears: owing to the pressure hysteresis, the interfacial γ phase already formed would contain insufficient H to transform to β phase and too much H to relax to α phase without a change in the local temperature, which was tightly controlled by the sample arrangement. Positions in the sample closer to the hydrogen inlet (Fig. 3) showed no residual γ phase. Interestingly, in non-kinetic in situ studies on large samples [15,20,21], we have never observed the gamma phase in neutron diffraction profiles recorded during an early hydrogenation cycle near room temperature under pseudo-equilibrium conditions, most likely because much smaller increments in pressure were applied, requiring less γ phase to accommodate the consequently slower transformation. Joubert et al. [30] found no γ phase at the ends of their roughly isobaric kinetic sequences, in which the transformation was driven to completion by a 15-bar hydrogen pressure, whereas we applied much smaller pressure drives which halted the transformation at an intermediate stage, owing to the limited amount of hydrogen available under the prevailing isochoral conditions. Some narrow γ-like layer between coexisting α- and β-phase regions is possibly always necessary to accommodate the differences in lattice parameter between them but would be unobservable by diffraction if its relative volume were very small and if, as is likely, the layer were highly strained with widely distributed lattice parameters.

5. Conclusions

Carefully controlled experiments have shown that the γ phase genuinely coexists with both the α and β phases at nanoscopic scales under isothermal conditions during the α–β phase transformation in the $LaNi_5$–H_2 system. Formation of the γ phase is an essential sequential step in the mechanism of the phase transformation near room temperature. The γ phase partially accommodates the large change in unit cell volume between the α and β phases with non-constant lattice parameters, demonstrating at least partial coherence of the transformation. The question of how the γ phase is stabilised by hydrogenating the sample at temperatures above about 80 °C remains to answered by further work.

Acknowledgements

Use of the ChemMatCARS sector 15 at the Advanced Photon Source was supported by the Australian Synchrotron Research Program, funded by the Commonwealth of Australia under the Major National Research Facilities Program. ChemMatCARS Sector 15 is principally supported by the U.S. National Science Foundation/Department of Energy under grant number CHE0087817. The Advanced Photon Source is supported by the U.S. Department of Energy, Basic Energy Sciences, Office of Science, under Contract No. W-31-109-Eng-38. The authors are grateful to Prof. E. Akiba for supplying the high-quality $LaNi_5$ used in this study.

References

[1] P. Fischer, A. Furrer, G. Busch, L. Schlapbach, Helv. Phys. Acta 50 (1977) 421.
[2] A. Percheron-Guégan, C. Lartigue, J.-C. Achard, P. Germi, F. Tasset, J. Less-Common Met. 74 (1980) 1.
[3] P. Thompson, J.J. Reilly, L.M. Corliss, J.M. Hastings, R. Hempelmann, J. Phys. F: Met. Phys. 16 (1986) 675.
[4] J.L. Soubeyroux, A. Percheron-Guégan, J.-C. Achard, J. Less-Common Met. 129 (1987) 181.
[5] C. Lartigue, A. Le Bail, A. Percheron-Guégan, J. Less-Common Met. 129 (1987) 676.
[6] A.E.M. de Weirman, A.A. Staals, P.H.L. Notten, Philos. Mag. A 70 (1995) 837.
[7] G.-H. Kim, C.-H. Chun, S.-G. Lee, J.-Y. Lee, Acta Metall. Mater. 42 (1994) 3157.
[8] G.-H. Kim, S.-G. Lee, K.-Y. Lee, C.-H. Chun, J.-Y. Lee, Acta Metall. Mater. 43 (1995) 2233.
[9] T. Yamamoto, H. Inui, M. Yamaguchi, Mater. Sci. Eng. A 329–331 (2002) 367.
[10] H. Inui, T. Yamamoto, M. Hirota, M. Yamaguchi, J. Alloys Compd. 330–332 (2002) 117.
[11] K. Nomura, H. Uruno, S. Ono, H. Shimozuka, S. Suda, J. Less-Common Met. 107 (1985) 221.
[12] E.H. Kisi, C.E. Buckley, E.MacA. Gray, J. Alloys Compd. 185 (1992) 369.
[13] E. Wu, E.MacA. Gray, E.H. Kisi, J. Appl. Crystallogr. 31 (1998) 356.
[14] E. Wu, E.H. Kisi, E.MacA. Gray, J. Appl. Crystallogr. 31 (1998) 363.
[15] M.P. Pitt, E.MacA. Gray, E.H. Kisi, B.A. Hunter, J. Alloys Compd. 293 (1999) 118.
[16] R. Cěrný, J.-M. Joubert, M. Latroche, A. Percheron-Guégan, K. Yvon, J. Appl. Crystallogr. 33 (2000) 997.

[17] R. Černý, J.-M. Joubert, M. Latroche, A. Percheron-Guégan, K. Yvon, J. Appl. Crystallogr. 35 (2002) 288.
[18] E.H. Kisi, E. Wu, M. Kemali, J. Alloys Compd. 330–332 (2002) 202.
[19] E. Wu, E.MacA. Gray, D.J. Cookson, J. Alloys Compd. 330–332 (2002) 229.
[20] M.P. Pitt, E.MacA. Gray, B.A. Hunter, J. Alloys Compd. 330–332 (2002) 241.
[21] E.H. Kisi, E.MacA. Gray, S.J. Kennedy, J. Alloys Compd. 216 (1994) 123.
[22] P.H.L. Notten, J.L.C. Daams, R.E.F. Einerhand, J. Alloys Compd. 210 (1994) 223.
[23] Y. Fukai, The Metal–Hydrogen System, Springer–Verlag, Berlin, 1993, p. 2.
[24] S. Ono, K. Nomura, E. Akiba, H. Uruno, J. Less-Common Met. 113 (1985) 113.
[25] T. Matsumoto, A. Matsushita, J. Less-Common Met. 123 (1986) 135.
[26] E. Akiba, K. Nomura, S. Ono, J. Less-Common Met. 129 (1987) 159.
[27] F.A. Kuijpers, B.O. Loopstra, J. Phys. Chem. Solids 35 (1974) 301.
[28] G.D. Sandrock, J.J. Murray, M.L. Post, J.B. Taylor, Mater. Res. Bull. 17 (1982) 887.
[29] A. Yoshikawa, Y. Uyenishi, H. Iizumi, T. Matsumoto, N. Takano, F. Terasaki, J. Alloys Compd. 280 (1998) 204.
[30] J.-M. Joubert, R. Černý, M. Latroche, A. Percheron-Guégan, B. Schmitt, Acta Mater. 54 (2006) 713.
[31] E.H. Kisi, E.MacA. Gray, J. Alloys Compd. 217 (1995) 112.
[32] M. Pons, P. Dantzer, Z. Phys. Chem. 183 (1994) 225.
[33] E.MacA. Gray, C.E. Buckley, E.H. Kisi, J. Alloys Compd. 215 (1994) 201.
[34] E.MacA. Gray, D.J. Cookson, T.P. Blach, J. Appl. Crystallogr. 39 (2006) 850.
[35] B.A. Hunter, Int. Union of Crystallogr. Commission on Powder Diffraction Newsletter 20 (1988) 21, available at URL www.iucr.org/iucr-top/comm/cpd/Newsletters/no20summer1998/art15/art15.htm.
[36] V.A. Yartys, V.V. Burnasheva, K.N. Semenenko, N.V. Fadeeva, S.P. Solov'ev, Int. J. Hydrogen Energy 7 (1982) 957.